A Versatile Simulation Method for Complex Single Mixed Refrigerant Natural Gas Liquefaction Processes

Matias Vikse,[†] Harry A. J. Watson,[‡] Truls Gundersen,[†] and Paul I. Barton[*,‡]

†*Department of Energy and Process Engineering, Norwegian University of Science and Technology (NTNU), Trondheim, Norway*

‡*Process Systems Engineering Laboratory, Massachusetts Institute of Technology, Cambridge MA, USA*

E-mail: pib@mit.edu

Abstract

Natural gas liquefaction is an energy intensive process with very small driving forces particularly in the low temperature region. Small temperature differences in the heat exchangers and high operating and capital costs require the use of an accurate and robust simulation tool for analysis. Unfortunately, state-of-the-art process simulators such as Aspen Plus and Aspen HYSYS have significant limitations in their ability to model multistream heat exchangers, which are critical unit operations in liquefaction processes. In particular, there exist no rigorous checks to prevent temperature crossovers from occurring in the heat exchangers, and the parameters must therefore be determined through a manual iterative approach in order to establish feasible operating conditions for the process. A multistream heat exchanger model that performs these checks, as well as area calculations for economic analysis, has previously been developed using a nonsmooth modeling approach. In addition, the model was used to

successfully simulate the PRICO process with the Peng-Robinson equation of state. However, the PRICO process is one of the most basic single mixed refrigerant processes, and it is therefore necessary to investigate whether the nonsmooth framework is capable of also simulating larger and more complex single mixed refrigerant processes. In this article, the nonsmooth multistream heat exchanger model is used to simulate three different single mixed refrigerant processes of varying complexity. Different case studies are performed, each solving for a different set of unknown variables. Several different variables were considered in the analysis to investigate whether the models obtained feasible solutions even for ostensibly challenging cases such as varying the mixed refrigerant composition. The solutions are then validated using results from Aspen Plus and Aspen HYSYS. The simulations in Aspen Plus gave nearly identical solutions to the nonsmooth models. Results in HYSYS, on the other hand, correlated well at high temperatures but deviated from the nonsmooth solution at cold temperatures. The disparity was caused by different ideal gas enthalpy correlations used by the two simulation tools.

Introduction

Liquefied natural gas (LNG) plays an important role in the global shift towards green energy sources. It is considered a cleaner alternative to oil and coal due to its low sulfur content, lower CO_2 emissions and lack of particle emissions, while at the same time avoiding the transportation difficulties associated with traditional pipeline gas. However, the liquefaction of natural gas is a very energy intensive process that requires cooling to about -162°C. Investments in expensive, custom and proprietary technology such as cryogenic heat exchangers and turbomachinery are necessary, and along with the high operating costs, liquefaction accounts for about 30-40% of the total cost in the LNG chain.[1] LNG production plants are normally categorized into three types: base-load, peak-shaving and small-scale plants. Single mixed refrigerant (SMR) liquefaction processes are mainly considered for small-scale

and peak-shaving LNG production where capital costs rather than operational costs are of primary concern. The simplest SMR process is the Poly-Refrigerated Integrated Cycle Operations (PRICO) process, which consists of one multistream heat exchanger (MHEX) and a simple vapor-compression refrigeration cycle. SMR processes require fewer pieces of equipment than cascade processes at the expense of needing higher refrigerant flowrates and thus greater compression power.[2] Compactness of the design and the small equipment inventory also make SMR processes attractive for floating LNG (FLNG) systems.

Large temperature ranges and small temperature differences at cryogenic temperatures make liquefaction processes notoriously hard to analyze. The small driving forces are a consequence of heat exchange at cryogenic temperatures where thermodynamic irreversibilities become significant. Small inaccuracies in the process model at such low temperatures will propagate into significant exergy losses in the actual process that must be covered by additional compression power. The high operating and capital costs, as well as small temperature differences, require the use of an accurate and robust simulation tool for analyzing LNG processes. Nevertheless, state-of-the-art process simulators such as Aspen Plus[3] and Aspen HYSYS[4] suffer from significant limitations in the modeling of MHEXs, which constitute the core of LNG processes. For instance, Kamath et al.[5] and Watson et al.[6] experienced that commercial software such as Aspen Plus lacked rigorous checks for avoiding temperature crossovers in the MHEXs. Instead, suitable parameters had to be determined through a manual iterative trial-and-error approach to MHEX simulation. Due to these limitations of conventional process simulators, attempts have been made at modeling MHEXs in a way that inherently avoids solutions with temperature crossovers.

Many different modeling approaches for MHEXs have been proposed in the literature. Hasan et al.[7,8] developed a model using a superstructure of two-stream heat exchangers and then solving a heat integration (HI) problem with no external utilities. Their model can handle phase changes in the MHEX as long as the phases traversed are known a priori. The result is a mixed-integer nonlinear program (MINLP) that is computationally expensive to

solve, and requires global optimization to guarantee a correct solution.

Recently, Rao and Karimi[9] proposed an alternative superstructure that handles unknown inlet/outlet stream states without introducing boolean variables. The model represents the MHEX as a series of stream bundles defined using a superstructure of two-stream heat exchangers. Nonlinear constraints are included to ensure that phase boundaries occur at the endpoints of each heat exchanger such that it operates within a specific phase regime. A process simulator (e.g. Aspen Plus) is used for calculating the stream properties in the model. The final model is a nonconvex NLP that is laborious to solve, particularly due to the repeated property evaluations done by the process simulator, and again requires global optimization methods. However, if explicit property correlations are used instead, boolean variables must be added to the model, resulting in an MINLP.

Kamath et al.[5] proposed another MHEX model, borrowing heavily from the concepts of pinch analysis (PA) and composite curves. However, rather than solving a network synthesis problem using a superstructure approach, the authors perform energy targeting using the simultaneous optimization and heat integration procedure originally proposed by Duran and Grossmann.[10] The result is a fully equation-oriented (EO) model where phase changes are handled using a disjunctive model represented in terms of complementarity constraints. Unlike the model by Hasan et al.,[7,8] the inlet and outlet phase regimes of the streams need not be known a priori and may be solved for as part of the simulation. Nonetheless, MHEX simulation still requires solving a nonconvex optimization problem involving complementarity constraints, which violate most conventional constraint qualifications.

Pattison and Baldea[11] developed an alternative MHEX model using a pseudo-transient EO approach. The model assumes that the relative sequence of stream temperatures is known (and fixed) prior to simulation to construct a series of enthalpy intervals for the composite curves. Each enthalpy interval may be split further into segments to improve the accuracy of calculations, especially in the two-phase region where thermal properties of the fluids are highly nonlinear functions of temperature. The temperatures for each

enthalpy interval are then calculated from thermophysical property models by introducing a nonphysical time-dependent temperature variable, and the resulting model is expressed as a system of differential-algebraic equations (DAEs). The pseudo-transient MHEX model is capable of handling phase changes while avoiding the use of either disjunctive programming or boolean variables. Instead, phase transitions are handled by perturbing the time variable across the kink while keeping the temperature constant. The properties are then resolved using the solution at the previous time step as an initial guess.

The literature on MHEX modeling and design for LNG processes mainly centers around flowsheet optimization. The models by Hasan et al.,[7,8] Rao and Karimi,[9] Kamath et al.[5] and Pattison and Baldea[11] all involve solving nonconvex optimization models, sometimes to global optimality, where the minimum approach temperature constraints are enforced as part of the optimization. Although flowsheet optimization is an essential tool in developing cost and energy efficient process designs, process simulation also provides a powerful tool in the engineering toolbox. In particular, process simulation allows engineers to study existing systems that are not necessarily optimal. Furthermore, it can be used to probe the behavior and sensitivity of the system in a neighborhood of the current operating point to reveal relatively simple and cost effective improvements that require no additional investments. Process simulation by solving a nonlinear equation system is also significantly less computationally expensive than solving a nonconvex optimization problem, and is thus preferred when a feasible rather than optimal design is sought. Also, a reliable simulation model can be be extremely useful in providing feasible initial guesses to an optimization code, usually enhancing the reliability of the optimization.[12] Moreover, the problem with temperature crossovers in the MHEXs observed in Aspen Plus and Aspen HYSYS is more challenging in the context of simulation due to the absence of a minimum approach temperature constraint. A MHEX model capable of imposing feasible heat transfer without including additional constraints is the MHEX model developed by Watson et al.[6,13] The model employs new advances in nonsmooth analysis for handling composite curves, phase transitions and area calculations.

No boolean variables or disjunctive representations are used for identifying the temperature or state of the stream segments. Instead, the model applies nonsmooth mathematical operators such as min, max and mid. Similar to the models by Kamath et al.[5] and Pattison and Baldea,[11] the nonsmooth MHEX model is based on composite curves and the concepts of PA. The result is a nonsmooth algebraic equation system that can be solved using a nonsmooth Newton-type solver. Furthermore, one of the nonsmooth equations contains a reformulation of the Duran and Grossmann[10] simultaneous optimization and heat integration model, and is used for constraining the minimum approach temperature. Consequently, the model is capable of simulating MHEXs while avoiding the problem of temperature crossovers, and has already been used to simulate the PRICO process successfully.[6,14] However, the PRICO process is the most basic industrially relevant SMR process, and thus the objective of this article is to investigate whether the model is capable of simulating larger and more commercially interesting processes.

Background

The MHEX model

The nonsmooth MHEX model developed by Watson et al.[6] is a natural generalization of the classical two-stream countercurrent heat exchanger model. The standard two-stream heat exchanger model is given by Equations (1)-(3), which are the energy balance, the definition of the minimum temperature difference ΔT_{min}, and the statement of the physical ability of the equipment to transfer heat, respectively:

$$mC_{\mathrm{p,H}}\left(T_{\mathrm{H}}^{\mathrm{IN}} - T_{\mathrm{H}}^{\mathrm{OUT}}\right) = mC_{\mathrm{p,C}}\left(T_{\mathrm{C}}^{\mathrm{OUT}} - T_{\mathrm{C}}^{\mathrm{IN}}\right), \tag{1}$$

$$\Delta T_{\mathrm{min}} = \min\left\{T_{\mathrm{H}}^{\mathrm{IN}} - T_{\mathrm{C}}^{\mathrm{OUT}}, T_{\mathrm{H}}^{\mathrm{OUT}} - T_{\mathrm{C}}^{\mathrm{IN}}\right\}, \tag{2}$$

$$UA = \frac{Q}{\Delta T_{\mathrm{LM}}}, \tag{3}$$

where $mC_{\mathrm{p,H/C}}$ are the heat capacity flowrates for the hot (H) and cold (C) streams (assumed to be constant), U is the overall heat transfer coefficient, A is the heat exchanger area, $Q \equiv mC_{\mathrm{p,H}}\left(T_{\mathrm{H}}^{\mathrm{IN}} - T_{\mathrm{H}}^{\mathrm{OUT}}\right)$ is total heat transferred and ΔT_{LM} is the log-mean temperature difference.

The energy balance can be extended to the case of n_{H} hot and n_{C} cold streams as follows:

$$\sum_{i=1}^{n_{\mathrm{H}}} mCp_{\mathrm{H},i}\left(T_{\mathrm{H},i}^{\mathrm{IN}} - T_{\mathrm{H},i}^{\mathrm{OUT}}\right) = \sum_{j=1}^{n_{\mathrm{C}}} mCp_{\mathrm{C},j}\left(T_{\mathrm{C},j}^{\mathrm{OUT}} - T_{\mathrm{C},j}^{\mathrm{IN}}\right). \tag{4}$$

Similarly, an equation for the total heat exchanger area was included for the MHEX case by considering vertical heat exchange (matching) within enthalpy intervals k of the hot and cold composite curves

$$UA = \sum_{k=1}^{K-1} \frac{\Delta Q^k}{\Delta T_{\mathrm{LM}}^k}. \tag{5}$$

Here, K is used to denote the total number of enthalpy intervals and ΔQ^k is the enthalpy change of the interval.

The minimum approach temperature constraint, however, cannot readily be generalized to the case of multiple streams. In a two-stream heat exchanger, the minimum temperature difference occurs at either endpoints of the heat exchanger provided the mC_{p} terms are constant. However, in MHEXs the minimum temperature difference can occur at any of the stream inlets, which are not necessarily located at the endpoints of the composite curves. Therefore, in order to prevent temperature crossovers, Watson et al.[6] treat the heat exchanger as a HI problem with no external utilities and solve for the ΔT_{min} variable using a reformulation of the simultaneous optimization and heat integration model by Duran and Grossmann.[10] Their formulation is compactly expressed as follows:

$$\min_{p \in P}\{EBP_{\mathrm{C}}^p - EBP_{\mathrm{H}}^p\} = 0, \tag{6}$$

where P is the (finite) set of candidate pinch points and $EBP_{\mathrm{H/C}}^p$ are the enthalpies of

extended hot/cold composite curves for pinch candidate p as defined in Watson et al.[6]

In liquefaction processes, the streams in a MHEX are multicomponent and normally undergo phase changes. In the single-phase regimes, the fluid composition will remain constant and the heat capacity flowrates can be approximated as constant without a significant loss in accuracy. During phase change, however, there is generally a highly nonlinear variation in the enthalpy as function of temperature. A critical issue in heat exchanger modeling is handling the nonsmooth change in physical properties at the phase boundaries. This is of particular importance in MHEX models where the stream phases are normally not known prior to simulation. Rather than using boolean variables or a disjunctive representation followed by solving a nonconvex optimization problem, Watson and Barton[13] presented a nonsmooth formulation using the mathematical operators min, max and mid to identify the correct temperature and phase of the streams, where the mid operator is a function that maps to its median argument. Each process stream is subdivided into superheated (sup), two-phase (2p) and subcooled (sub) substreams whose inlet and outlet temperatures are calculated from the following equations:

$$T_{\text{sup}}^{\text{in/out}} = \max\left(T_{\text{DP}}, T^{\text{IN/OUT}}\right), \tag{7}$$

$$T_{\text{2p}}^{\text{in/out}} = \text{mid}\left(T_{\text{DP}}, T_{\text{BP}}, T^{\text{IN/OUT}}\right), \tag{8}$$

$$T_{\text{sub}}^{\text{in/out}} = \min\left(T_{\text{BP}}, T^{\text{IN/OUT}}\right), \tag{9}$$

where $T^{\text{IN/OUT}}$ are the inlet/outlet temperatures of the process stream, $T_{\text{sub/2p/sup}}^{\text{in/out}}$ are the inlet/outlet temperatures to the subcooled/two-phase/superheated substreams, and T_{DP} and T_{BP} are the dew point and bubble point temperatures of the process streams, respectively. Each substream may be partitioned further into affine stream segments with constant heat capacity flowrate to improve the accuracy of calculations over large temperature ranges. Examples presented by Watson et al.[14] show that using less than 20 segments to represent the two-phase region for the PRICO process can lead to significant inaccuracy in the simulations

resulting in an under-prediction of the necessary compression power. The target temperature of each stream segment in this region is calculated using pressure-enthalpy (PQ-)flashes over equidistant enthalpy intervals. Additionally, as stream properties and thus the phase boundaries change during simulation, the flash algorithms used in these simulations must be capable of handling instances of single phase flow within the nonsmooth framework. This is particularly important for modeling the process equipment (i.e. valves and compressors) that handle streams leaving the MHEX in unknown a priori phase regimes.

For simple thermodynamic models, the necessary robustness of the flash calculations can be accomplished through a nonsmooth reformulation of the well-known Rachford-Rice equation:[13,15]

$$\operatorname{mid}\left\{\alpha, \alpha-1, -\sum_{i=1}^{n_c} \frac{z_i\left(K_i-1\right)}{1+\alpha\left(K_i-1\right)}\right\}=0. \tag{10}$$

In Equation (10), n_c is the total number of components, α is the vapor fraction, z_i is the feed mole fraction of component i and K_i is the equilibrium coefficient of component i. While Equation (10) works well for ideal or near-ideal property models, this formulation struggles for more complex equations of state (EOS) such as the Peng-Robinson cubic EOS.

Boston and Britt[16] came up with an inside-out algorithm for flash calculations, which has proven to be very dependable, and is still the primary algorithm used in state-of-the-art process simulation tools such as Aspen Plus. Rather than solving the flash equations directly, the inside-out algorithm first estimates the solution using simple models for calculating thermodynamic properties. Then, model parameters are updated in an outer loop using more rigorous relations. Nevertheless, the algorithm is based on the assumption that the solution will always be in the two-phase vapor-liquid region, which is problematic in instances such as simulation and optimization of LNG processes where the stream phases are normally not known a priori. Methods for post-processing the results to find the true single-phase answer exist. However, these methods can be computationally expensive and are often based on heuristics. Furthermore, the post-processing methods are susceptible to failure, particularly near the phase-boundaries as shown by Watson et al.[17] Therefore, a nonsmooth extension

of the Boston-Britt inside-out flash algorithm that handles phase-changes without relying on post-processing methods has been developed for use with nonideal property models. The procedure is summarized in a 3-paper series by Watson et al.,[14,17,18] where a mid function analogous to Equation (10) is employed for automatic outlet phase regime detection within the robust flash calculation procedure. The algorithm was shown to handle instances close to the phase-boundaries for which the conventional inside-out algorithm implemented in Aspen Plus failed to detect the correct single-phase.[17] Furthermore, Watson et al.[14] presented a method for calculating correct generalized sensitivity information from the nonsmooth equation system, allowing the flash calculations to be included as nested subroutines in flowsheet models. This results in a reduced model size and increased robustness compared to fully EO process models, especially when a large number of stream segments are used for representing the two-phase region.

Solving nonsmooth equation systems

The MHEX model requires solving a nonsmooth algebraic equation system. Traditionally, this has been regarded as a hard problem due to the presence of undefined derivatives at points of nondifferentiability. One way of coping with nondifferentiability has been to use smooth approximations of nonsmooth functions such as the following from Balakrishna and Biegler[19] for the max operator:

$$\max\{0, f(x)\} \approx \frac{\left(\sqrt{f(x)^2 + \beta^2} + f(x)\right)}{2}. \tag{11}$$

However, the selection of the user defined parameter β is non-trivial and may lead to either an ill-conditioned approximation or loss of accuracy when poorly chosen.[20]

Alternatively, the nonsmooth equation system can be solved directly using a nonsmooth Newton-type method, where the following Newton step is used to generate the next iterate

$\mathbf{x}^{k+1}$:

$$\mathbf{G}(\mathbf{x}^k)(\mathbf{x}^{k+1} - \mathbf{x}^k) = -\mathbf{f}(\mathbf{x}^k). \tag{12}$$

Here, $\mathbf{G}(\mathbf{x}^k)$ is an element of a generalized derivative of $\mathbf{f}$ at the point $\mathbf{x}^k$. Equation (12) solves for the next iterate $\mathbf{x}^{k+1}$ provided the chosen element of the generalized derivative is nonsingular at $\mathbf{x}^k$. Singular generalized derivative elements may occur in the MHEX model due to residuals of the form $\min\{0, y\}$, which are used for solving Equation (6). In such cases, a Newton-type solver that is applicable to singular generalized derivative elements is the linear programming (LP) Newton method by Facchinei et al.,[21] which solves the following linear program upon every iteration:

$$\begin{aligned}
&\min_{\gamma,\mathbf{x}} \ \gamma \\
&\text{s.t.} \ \left\|\mathbf{f}(\mathbf{x}^k) + \mathbf{G}(\mathbf{x}^k)(\mathbf{x} - \mathbf{x}^k)\right\|_\infty \leq \gamma \min\left(\left\|\mathbf{f}(\mathbf{x}^k)\right\|_\infty, \left\|\mathbf{f}(\mathbf{x}^k)\right\|_\infty^2\right), \\
&\qquad \left\|(\mathbf{x} - \mathbf{x}^k)\right\|_\infty \leq \gamma \left\|\mathbf{f}(\mathbf{x}^k)\right\|_\infty, \\
&\qquad \mathbf{x} \in X,
\end{aligned} \tag{13}$$

where X is a polyhedral set of bounds on the problem and γ is a supplementary variable to drive convergence towards the solution. Moreover, the next iterate $\mathbf{x}^{k+1}$ is given by the $\mathbf{x}$ part of the solution. Fischer et al. showed that the LP Newton method can be adapted to ensure global convergence for continuously differentiable $\mathcal{C}^1$ and piecewise differentiable $\mathcal{PC}^1$ functions by including a backtracking line search.[22]

The authors have experienced that the LP Newton method may still take poor quality steps when $\mathbf{G}(\mathbf{x})$ is singular. A possible explanation is that an ill-conditioned generalized derivative causes the LP Newton method to take an aggressive step in a direction that does not lead to reduction of the norm of the function residual, which may lead to slow convergence or divergence of the iterates. However, by including the backtracking line search suggested by Fischer et al.,[22] the step length can be dampened appropriately, avoiding this issue altogether. The steps in the globalized LP Newton method are computationally expensive

compared to solving Equation (12). Therefore, in order to avoid excessive computing costs, a hybrid method is applied in these simulations, wherein Equation (12) is used when $\mathbf{G}(\mathbf{x})$ is nonsingular and well-conditioned, whereas the global LP Newton is applied otherwise.

The generalized derivative element $\mathbf{G}(\mathbf{x})$ is an extension of the classical derivative to certain classes of nondifferentiable functions. The Clarke Jacobian represents one such generalized derivative that is applicable to functions that are locally Lipschitz continuous on their domain.[23] A challenge with using elements of the Clarke Jacobian, however, is that these elements only follow calculus rules (e.g. the chain rule) as inclusions, and they are therefore impractical to calculate for most composite functions. The lexicographic (L-)derivative is another generalized derivative for functions that satisfy the conditions for lexicographic (L-)smoothness as described by Nesterov.[24] Khan and Barton[25] showed that L-derivatives are just as useful in nonsmooth numerical methods as elements of the Clarke Jacobian. The lexicographic directional (LD)-derivative is a generalization of the classic directional derivative that is computed sequentially along the directions indicated by the columns of a directions matrix $\mathbf{M}$. LD-derivatives follow calculus rules as equations and can be calculated for composite functions using an automatic differentiation (AD) framework.[26] Furthermore, the L-derivative can readily be obtained from the LD-derivative. A detailed review of evaluating LD-derivatives and their applications is provided by Barton et al.[27]

The nonsmooth functions in the MHEX model are piecewise differentiable ($\mathcal{PC}^1$) as defined by Scholtes,[28] and therefore satisfy the conditions for L-smoothness.[26] In addition, LD-derivatives of $\mathcal{PC}^1$ functions taken in the identity matrix directions are guaranteed to be elements of the function's Bouligand (B)-subdifferential.[26] B-subdifferential elements are also elements of the Clarke Jacobian and exhibit desirable properties in nonsmooth equation solving methods such as local second-order convergence.[29]

Simulation cases and results

In this paper, three different SMR processes are studied. The first example deals with an SMR liquefaction process consisting of one MHEX with two hot and two cold refrigerant streams working in different temperature ranges. The second example looks at an extended PRICO process with two MHEXs and NGL extraction after precooling. The third example considers a hybrid version of the two previous processes that considers both multiple refrigerant streams and NGL extraction after precooling. All simulations are carried out using the Peng-Robinson EOS with property parameter values taken from Aspen Plus. The models are written in the Julia v0.6.0 programming language and run on a Dell Latitude E5470 laptop in the Ubuntu v16.10 environment with an Intel Core i7-6820HQ CPU at 2.7 GHz and 8.2 GB RAM. Five stream segments are used for representing the physical streams in single-phase vapor/liquid regions and 20 stream segments for the two-phase region. The latter was chosen carefully to ensure accurate representation in accordance with Watson et al.[14] The tolerance for flowsheet convergence was set to $\|\mathbf{y}\|_\infty < 10^{-6}$, where $\mathbf{y}$ are the equation residuals, and the tolerance for the flash calculations was set to $\|\mathbf{y}\|_\infty < 10^{-8}$. The flash calculations are performed using the nonsmooth inside-out algorithm from Part 1 of Watson et al.[17] with the nonsmooth density extrapolation from Part 3.[18] Correct sensitivities are calculated using the methodology described in Part 2 of Watson et al.[14] As the flash calculations are nested in the flowsheet, the number of segments chosen for the two-phase region does not impact the model size. Furthermore, Equation (6) places a single constraint on the problem regardless of the number of stream segments used in the problem.

Case studies are performed to investigate whether the models are robust enough to obtain feasible solutions for different sets of unknown variables. Two cases are considered in the first two examples, whereas in the last example, three cases are studied. The variables considered in the analysis are the outlet temperatures of the high and low pressure refrigerant streams, pressure levels, refrigerant compositions, minimum temperature difference in the MHEXs, heat exchanger areas, and the NGL extraction temperature. Some of these variables, such as

the refrigerant composition and NGL extraction temperature, are more difficult to solve for as they influence several parts of the flowsheets. For the last two examples, validation of the results are performed in Aspen Plus using the same property parameters and thermo-physical property package. Comparisons are also done with results from Aspen HYSYS. However, it is important to observe that this does not mean that Aspen could have performed these simulations. Actually, Aspen Plus fails to converge for any of the following cases with the design specifications and initial guesses provided for Examples 2 and 3 in the Supporting Information. Their MHEX models are limited to one degree of freedom from solving the overall energy balance and can thus only handle a single unknown variable. The nonsmooth MHEX model, on the other hand, provides either two or three degrees of freedom depending on whether area calculations are included. Moreover, a ΔT_{min} or UA-value can be specified in the model, something that is not available for simulations in Aspen Plus, which instead calculates these parameters automatically for the given composite curves. Therefore, Aspen Plus is merely used for validating the physical feasibility of the solutions by providing the data from the result of the nonsmooth simulation, with the exception of the outlet temperature of the LPR stream in each MHEXs, which is calculated by Aspen Plus or Aspen HYSYS from the energy balance. The following nomenclature is used for the parameters and variables related to the MR streams in the model:

- Pressure level of the high pressure refrigerant: P_{HPR}.
- Pressure level of the low pressure refrigerant: P_{LPR}.
- Inlet/outlet temperatures of the high pressure refrigerant: $T_{\text{HPR}}^{\text{IN/OUT}}$.
- Inlet/outlet temperatures of the low pressure refrigerant: $T_{\text{LPR}}^{\text{IN/OUT}}$.
- Molar flowrate of the refrigerant: F_{MR}.
- Molar flowrate of refrigerant component i: $f_{\text{MR},i}$.

Example 1

In this example, a modified PRICO process is considered in which the high pressure refrigerant (HPR) is separated into a liquid and vapor branch. The liquid branch (Branch 1) is subcooled to a temperature $T_{\mathrm{HPR},1}^{\mathrm{OUT}}$ before it is throttled to pressure level P_{LPR} and mixed with the low pressure refrigerant (LPR) stream to provide precooling. The vapor branch (Branch 2), on the other hand, is condensed and subcooled to a temperature $T_{\mathrm{HPR},2}^{\mathrm{OUT}}$ and then throttled to the same pressure P_{LPR} to provide cooling at the cold end of the MHEX. Figure 1 shows the flowsheet of this modified PRICO process. The configuration of the MHEX is similar to that of a spiral-wound heat exchanger (SWHX). The SWHX is a cryogenic heat exchanger, commonly used in Dual Mixed Refrigerant (DMR) processes, that consists of one or several stream bundles wound around a mandrel. Separate tubes are used for the hot refrigerant and natural gas streams, whereas the cold refrigerant is flowing countercurrently outside the bundles. Furthermore, different refrigerants may be used to provide cooling at different temperature levels, which results in less refrigerant that is circulated in the cold end of the heat exchanger. As a consequence, the heat transfer area required to cool the same quantity of natural gas is comparatively smaller.

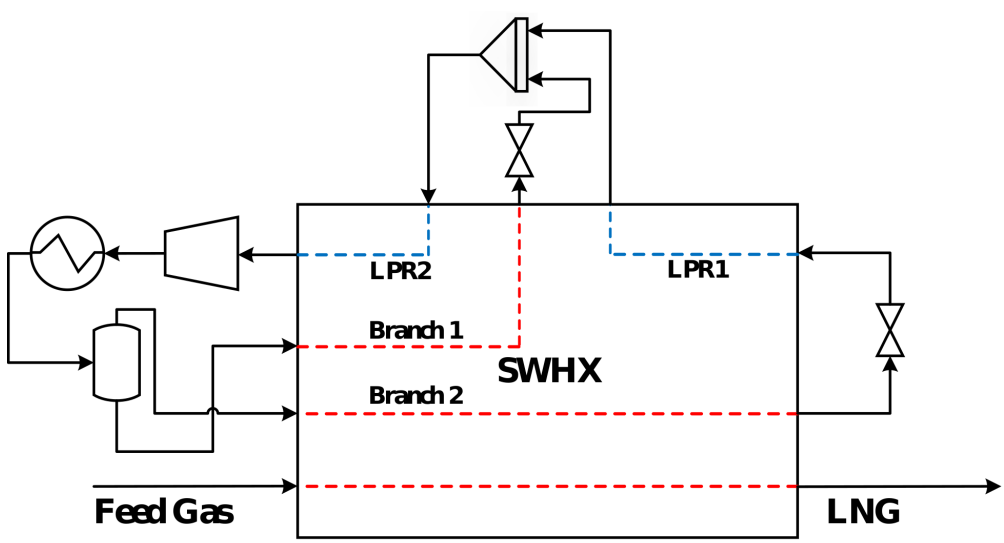

Figure 1: SMR process with a SWHX.

The SWHX is modeled as a single five-stream MHEX; a cold stream in the hot and cold end of the heat exchanger in addition to the three hot streams. The first LPR stream (LPR1) corresponds to the cold end of the SWHX and will have the same composition and flowrate as the vapor stream in Branch 2. This stream will leave the cold end of the SWHX at a temperature $T_{\mathrm{LPR},1}^{\mathrm{OUT}}$ where it is mixed with the liquid stream from Branch 1 to form the LPR2 stream. The LPR2 stream provides necessary precooling for the hot streams in the hot end of the SWHX and will exit the heat exchanger to enter the compressor at $T_{\mathrm{LPR},2}^{\mathrm{OUT}}$. The sets of unknown variables considered for this example are:

- **Case I - variable set**: P_{HPR}, P_{LPR}, UA.
- **Case II - variable set**: $f_{\mathrm{MR,ethane}}$, $T_{\mathrm{LPR},2}^{\mathrm{OUT}}$, ΔT_{min}.

Table S1 in the supporting information provides the initial guesses for the unknown variables and the values of the known parameters in the simulations. The model consists of 43 variables: the three variables solved for in each case as well as the temperatures for each stream segment in the subcooled and superheated regions. The temperatures for the segments in the two-phase region are solved sequentially in the nested subroutines and thus do not appear in the overall model. Nevertheless, only the parameters presented in Table S1 need to be provided by the user, while the remaining temperatures are calculated through an automatic initialization procedure that assumes a linear relationship between enthalpy and temperature in the subcooled and superheated phase regions.[14] For comparison, the PRICO model from Watson et al.[14] consists of 27 variables. The data for the natural gas stream are presented in Table S2 in the supporting information and are assumed fixed throughout this example. No tear equations are required in this model as the pressure levels, material flows and compositions are set for the high and low pressure refrigerant streams similar to an equation oriented approach. In addition, the temperature is fixed after the cooler. The results of the simulations are discussed for each of the two variable sets below.

Case I. Here, the minimum approach temperature ΔT_{min} remains fixed at 1.5 K while

varying the pressure levels of the refrigerant and the UA value. The high pressure level affects the split fraction in the separator and hence the refrigerant composition in the two branches. Consequently, it affects the shape of the composite curves and is more strenuous to solve for than in the original PRICO process. Flowsheet convergence was reached after 3 iterations and a total simulation time of 20.97 seconds including initialization. A solution is found with $P_{\mathrm{HPR}} = 1.5326$ MPa, $P_{\mathrm{LPR}} = 0.1855$ MPa and $UA = 9.29$ MW/K, which corresponds to a required isentropic compression power of 15.81 MW. Figure 2a shows the composite curves for the process and Figure 2b presents the driving force plot. The driving force plot shows that the process is constrained mainly in the cold end and at the point of mixing, which results in smaller driving forces compared to what was observed for the PRICO process.[14] The corresponding compression power is therefore significantly smaller. It should be stated here that this is only a feasible solution resulting from simulating the process, and that flowsheet optimization is not carried out in this paper.

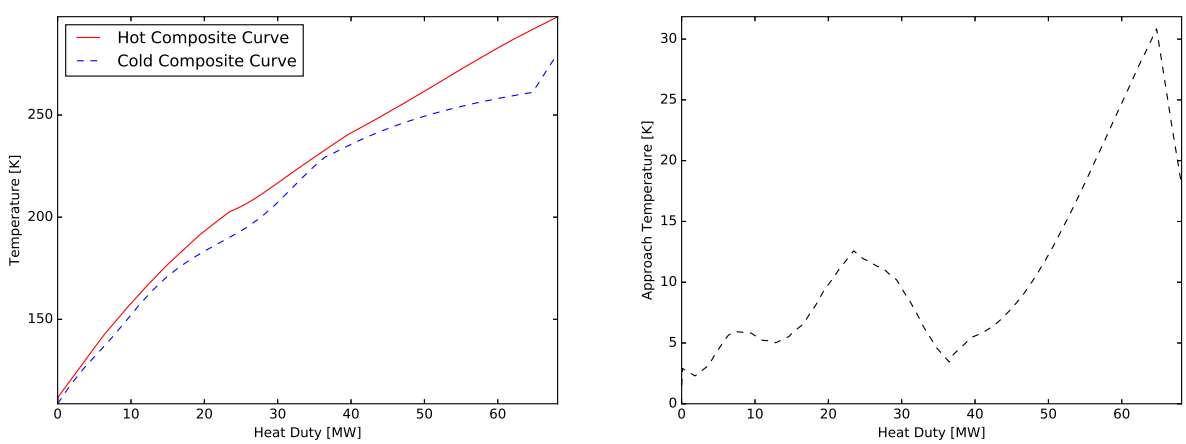

(a) (b)

Figure 2: (a.) Composite curves for Example 1, Case I. (b.) Corresponding driving force plot.

Case II. Here, the composition of the refrigerant mixture, the inlet temperature to the compressor and the minimum approach temperature are varied while keeping the UA-value fixed at 10 MW/K. The model solves for the refrigerant composition by varying the

molar flowrate of component i, here ethane, and then resolve the mole fractions $z_{\mathrm{MR},i}$ from $f_{\mathrm{MR},i} = z_{\mathrm{MR},i} F_{\mathrm{MR}}$. The simulation converged after 4 iterations requiring 31.2 seconds to solve including initialization of the stream variables. A solution is obtained with $T_{\mathrm{LPR},2}^{\mathrm{OUT}} = 271.30$ K, $\Delta T_{\mathrm{min}} = 1.59$ K, and a new refrigerant composition with 5.89 % nitrogen, 20.88 % methane, 38.63 % ethane and 34.62 % n-butane. The total MR flowrate is also changed from 2.928 to 2.892 kmol/s as a result of varying the component flowrate of ethane. The solution resulted in an isentropic compression power of 15.22 MW. Figure 3a shows the composite curves for the process and Figure 3b presents the driving force plot. A summary of the simulation results from the two cases are presented in Table 1.

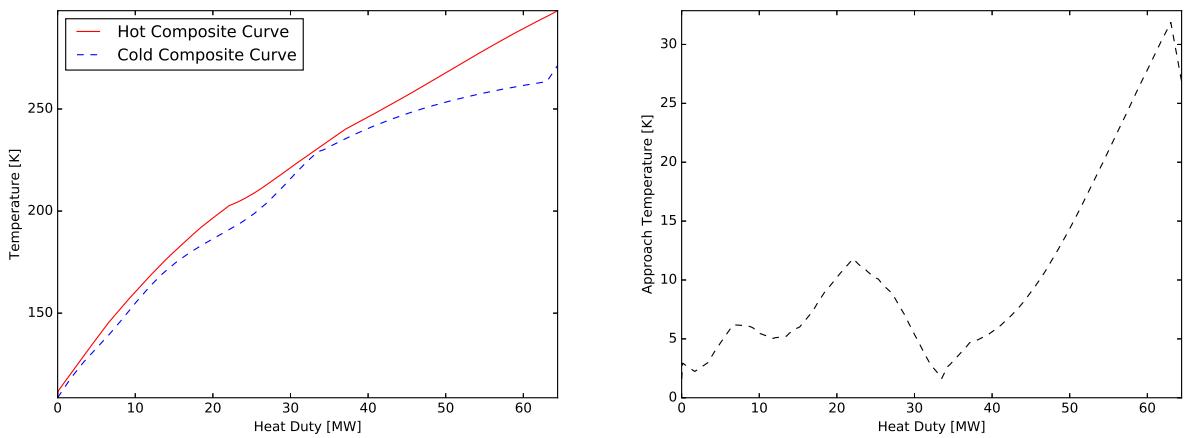

(a) (b)

Figure 3: (a.) Composite curves for Example 1, Case II. (b.) Corresponding driving force plot.

Example 1 represents a compact way of formulating the SWHX model, which is ideal when studying larger processes that include one or several SWHXs. The compact formulation reduces the number of variables in the model compared to using two separate MHEXs as required by Aspen HYSYS. A drawback with this formulation, however, is that the model only provides three degrees of freedom compared to six when using two MHEXs. As a consequence, more model parameters must be specified prior to simulation, thus removing some of the flexibility in the model. A similar process using two MHEXs that includes NGL

Table 1: Summary of simulation results for Example 1.

Property	**Case I**	**Case II**
Compression power [MW]	15.81	15.23
UA [MW/K]	9.29	10.00
ΔT_{min} [K]	1.50	1.57
F_{MR} [kmol/s]	2.928	2.890
P_{HPR} [MPa]	1.5326	1.7129
P_{LPR} [MPa]	0.1855	0.202
$T^{\text{OUT}}_{\text{LPR,2}}$ [K]	280.15	271.30
Composition [mol %]:		
Nitrogen	5.82	5.89
Methane	20.62	20.87
Ethane	39.37	38.63
n-Butane	34.19	34.61

extraction at intermediate temperatures is considered in Example 3.

Example 2

For LNG production that handles unprocessed feed gas, a key decision is whether to have integrated or upstream natural gas liquids (NGL) extraction. Heavier hydrocarbons freeze out at cold temperatures, which can cause plugging of process equipment. The LNG is also subject to quality constraints that may require heating value adjustments by removing heavier components. In addition, liquefied petroleum gas (LPG), i.e. propane and butane, is a valuable commodity and is therefore normally sold separately. This example deals with a modified PRICO process with two MHEXs and integrated extraction of natural gas liquids (NGLs). A rich natural gas is first precooled in MHEX 1 before separating the NGLs at an intermediate temperature to ensure an appropriate LNG composition. Figure 4 presents the process flowsheet. Unlike the process studied in Example 1, this model considers only one refrigerant composition in both exchangers.

The simulations in Example 2 use the same initial refrigerant composition, flowrate and low pressure level as Example 1. Again, this is not intended to indicate that these are optimal operation conditions, but rather to demonstrate the general simulation capabilities

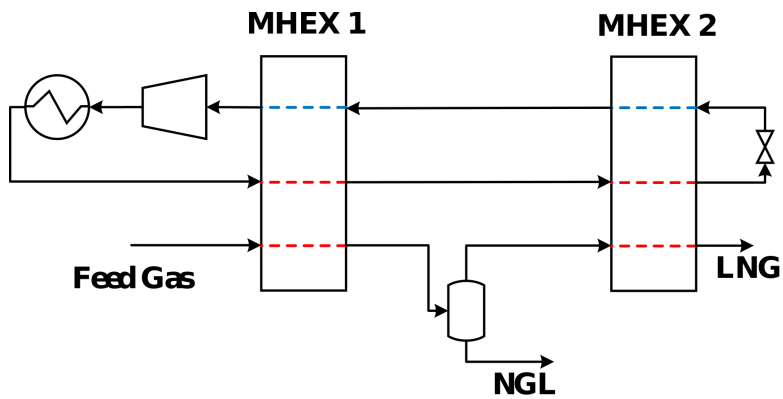

Figure 4: SMR process with NGL extraction

of the model. Other relevant process data are summarized in Table S3 in the supporting information. An MHEX model solving only Equations (4) and (6) was used for MHEX 1. Specifying either the UA-value or $\Delta T_{\min}$ as a parameter in this heat exchanger is challenging as they are dependent on the process conditions in MHEX 2 and vice versa. The MHEX design is also less critical for the precooler, where temperature driving forces are larger. Thus, an efficient approach is to use the two-equation MHEX model to first identify the approach temperature for a set of initial conditions, while calculating the required heat exchanger area subsequently. Then, in detailed design, the three-equation model can be employed to iterate around the initial area value as desired.

The model contains 53 variables, ten more than the model in Example 1. Table S4 in the supporting information presents the property data for the natural gas stream, which are held fixed in the simulations. A richer composition is used compared to Example 1 and the pressure is lowered from 5.5 MPa to 3.5 MPa to ensure adequate separation after precooling. In practical applications, the natural gas and hot refrigerant streams leave the MHEX at approximately the same temperature to avoid excessive subcooling of the refrigerant. Therefore, due to limited degrees of freedom in the simulation models, rather than varying the outlet temperatures of the natural gas stream and HPR refrigerant streams independently they are assigned to the same temperature variable. With two equations provided by MHEX 1 and three by MHEX 2, the model can solve for five variables involved in the

heat exchangers. The following two cases are studied in this paper:

- **Case I - variable set**: $f_{\text{MR,n-butane}}$, $\Delta T_{\text{min,MHEX1}}$, P_{LPR}, $T^{\text{OUT}}_{\text{LPR,MHEX2}}$, UA_{MHEX2}.
- **Case II - variable set**: P_{LPR}, $\Delta T_{\text{min,MHEX1}}$, P_{HPR}, $T^{\text{OUT}}_{\text{LPR,MHEX2}}$, $\Delta T_{\text{min,MHEX2}}$.

Case I. In this case, the refrigerant composition, the minimum approach temperature in MHEX 1, the low pressure level, the LPR temperature out of MHEX 2, and the UA value in MHEX 2 are varied, while keeping the approach temperature in MHEX 2 fixed. The flowsheet converged after 24.5 seconds and 4 iterations to a solution with $\Delta T_{\text{min,MHEX1}} = 8.00$ K, $P_{\text{LPR}} = 0.202$ MPa, $T^{\text{OUT}}_{\text{LPR,MHEX2}} = 209.91$ K and $UA_{\text{MHEX2}} = 7.57$ MW/K, resulting in an isentropic compression power of 15.19 MW. The new refrigerant composition and flowrate was found to be 5.96 % nitrogen, 21.12 % methane, 40.33 % ethane and 32.58 % n-butane with $F_{\text{MR}} = 2.916$ kmol/s. Furthermore, the natural gas composition after extraction is 1.18 % nitrogen, 90.35 % methane, 6.66 % ethane, 1.74 % propane, 0.03 % n-butane, 0.04 % iso-butane and 0.00 % iso-pentane. A UA_{MHEX1}-value of 3.07 MW/K was calculated during post-processing.

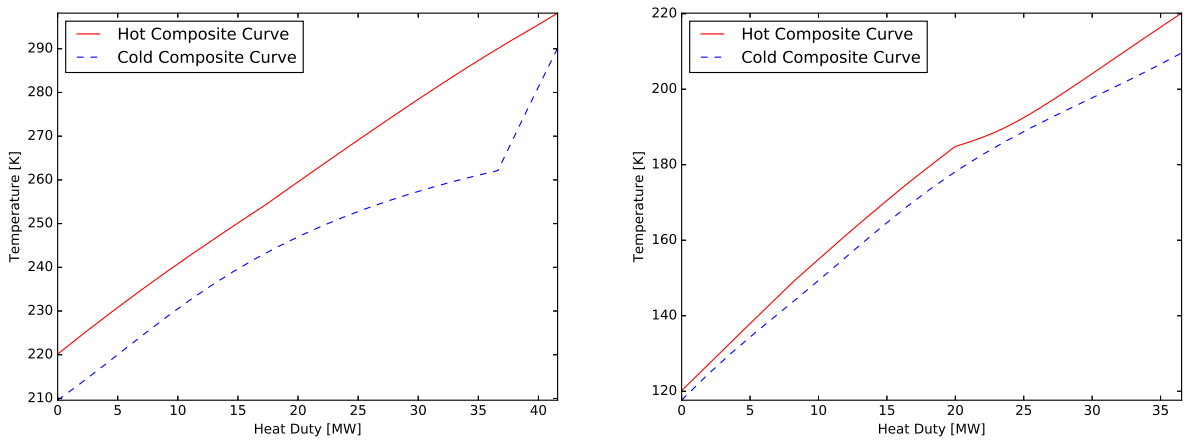

(a) (b)

Figure 5: (a.) Composite curves for MHEX 1 in Example 2, Case I. (b.) Corresponding for MHEX 2.

Figures 5 and 6 present the composite curves and the driving force plots for Case I. The driving force plot also includes results for the same case from simulations in Aspen Plus v9

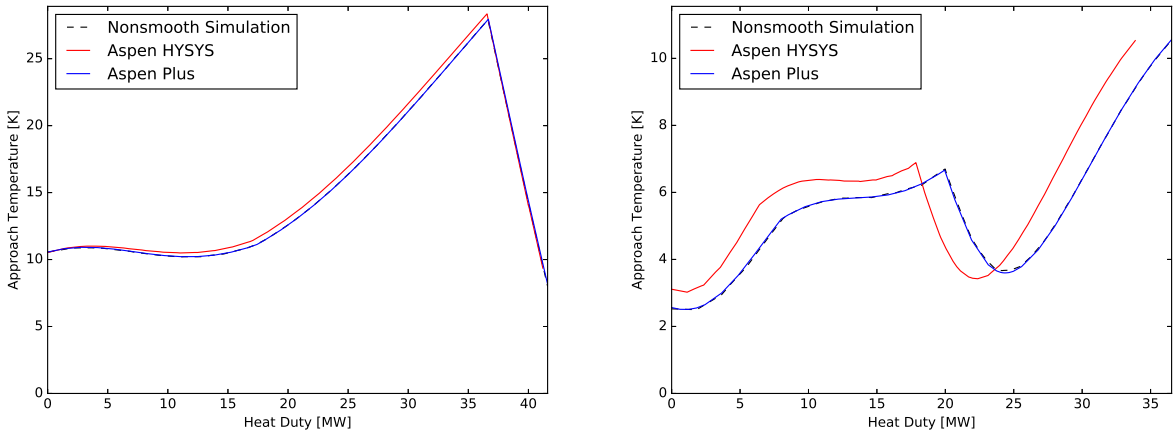

(a) (b)

Figure 6: (a.) Driving force plot for MHEX 1 in Example 2, Case I. (b.) Corresponding for MHEX 2.

and Aspen HYSYS v9 using 30 segments for each MHEX. As was mentioned earlier, both simulations were performed using the result from the nonsmooth model as a starting point and allowing the outlet temperature of the LPR stream in each MHEX to vary. Stream pressures cannot be selected as variables in the MHEX models in Aspen, and consequently they fail to solve for Case I and II in this example since fixing $T^{\mathrm{OUT}}_{\mathrm{HPR,MHEX1}}$ and $T^{\mathrm{OUT}}_{\mathrm{LPR,MHEX1}}$ would over-specify MHEX 1. Aspen Plus and the nonsmooth model obtain the same driving force distribution at the solution. In addition, the isentropic compression power, $UA_{\mathrm{MHEX1/2}}$ and $\Delta T_{\mathrm{min,MHEX2}}$ all lie within <1% of the results of the nonsmooth model, whereas $\Delta T_{\mathrm{min,MHEX1}}$ lies within <2%. A clear similarity can also be observed between the nonsmooth model and the solution from Aspen HYSYS, particularly in Figure 6a where the curves are almost identical. Nevertheless, the duty in MHEX 2 in HYSYS is shifted as a result of different ideal gas enthalpy correlations. HYSYS uses the Cavett equation for ideal gas enthalpy calculations, whereas Aspen Plus and the nonsmooth model both employ the ideal gas heat capacity equation (DIPPR 107) by Aly and Lee.[30] The effect of these enthalpy calculations are likely to be more critical at lower temperatures where a higher liquid content is present and the correlations are extrapolated. The temperature after the low temperature valve is 0.6 K

lower compared to Aspen Plus and the nonsmooth simulation. HYSYS found the isentropic compression power to be 15.11 MW, a <1% deviation from the result of the nonsmooth model. Larger deviations were observed for the two UA-values, particularly for UA_{MHEX2}. The large deviation in calculated UA-value for MHEX 2 is due to the shift in the driving force distribution curves and a larger driving force at the low temperature side of the exchanger (see Figure 6b). Table 3 presents the resulting MHEX and compressor data for the HYSYS simulation.

Case II. The second case solves for both pressure levels of the refrigerant, the minimum approach temperature in both MHEXs and the LPR temperature out of MHEX 2. The model converged after 5 iterations and a total simulation time (including initialization) of 24.9 seconds to the solution $\Delta T_{\mathrm{min,MHEX1}} = 8.00$ K, $\Delta T_{\mathrm{min,MHEX2}} = 2.33$ K, $P_{\mathrm{LPR}} = 0.2064$ MPa, $P_{\mathrm{HPR}} = 1.355$ MPa and $T^{\mathrm{OUT}}_{\mathrm{LPR,MHEX2}} = 211.72$ K. After post-processing, the UA-value of MHEX 1 was calculated to 3.68 MW/K. This solution requires 14.38 MW of isentropic compression power. Figures 7 and 8 show the composite curves and driving force plots for the solution. The driving force plots show that the solution of Case II exhibits comparatively smaller driving forces in MHEX 2 than Case I, resulting in the observed drop in compression power.

As in Case I, the model was simulated using Aspen Plus and Aspen HYSYS with the results from the nonsmooth model as inputs and letting the outlet temperature of the LPR vary. Figure 8 presents the driving force plots for both MHEXs, which display the same trend that was observed for Case I. Aspen Plus simulations yield identical driving force curves as for the nonsmooth model. Aspen HYSYS shows good correlation with the nonsmooth model at high temperatures. However, the curves are again shifted relative to one another in MHEX 2 as a result of the different ideal gas enthalpy calculation methods. The Aspen Plus validation results in a required isentropic compression power of 14.37 MW. In addition, the UA-values were calculated to be $UA_{\mathrm{MHEX1}} = 3.674$ MW/K and $UA_{\mathrm{MHEX2}} = 9.52$ MW/K, both within 1% of the results of the nonsmooth model. The minimum approach temperatures

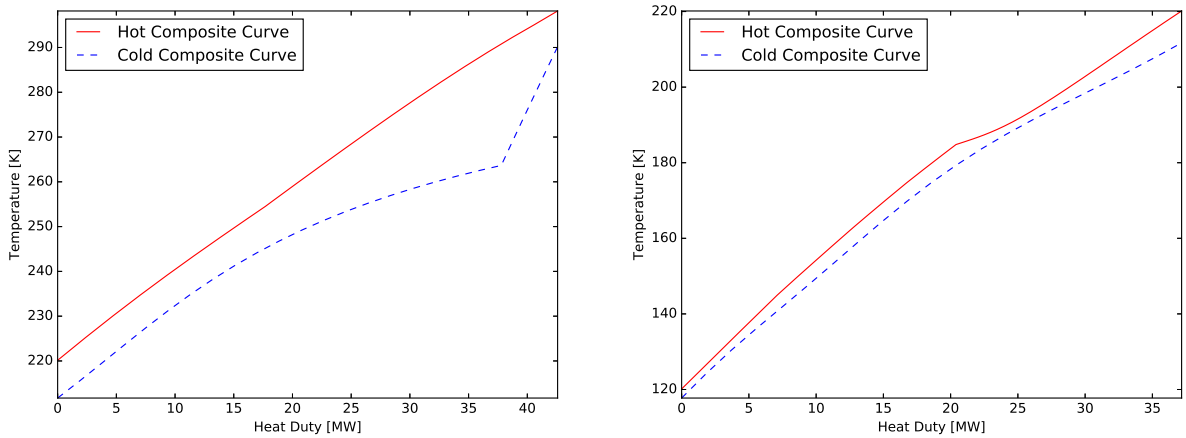

(a) (b)

Figure 7: (a.) Composite curves for MHEX 1 in Example 2, Case II. (b.) Corresponding for MHEX 2.

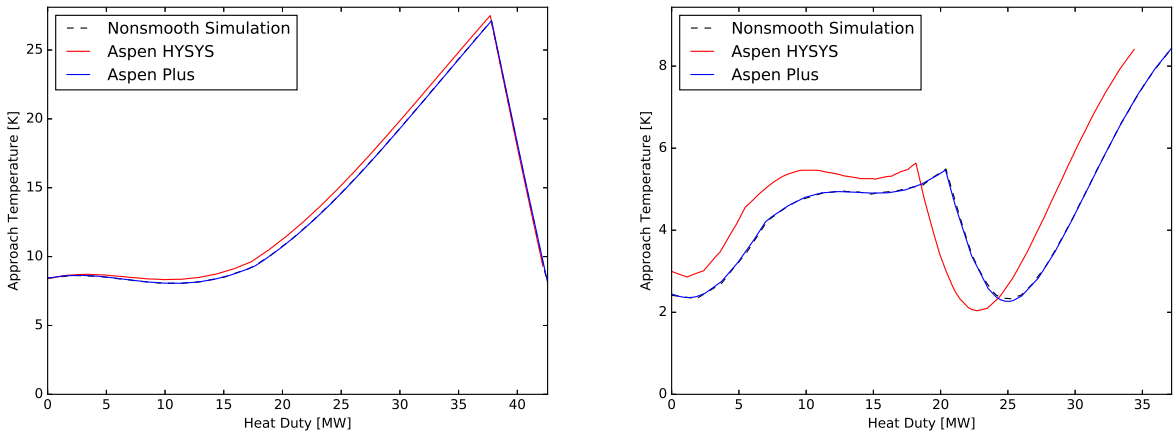

(a) (b)

Figure 8: (a.) Driving force plot for MHEX 1 in Example 2, Case II. (b.) Corresponding for MHEX 2.

were $\Delta T_{\text{min,MHEX1}} = 8.06$ K and $\Delta T_{\text{min,MHEX2}} = 2.27$ K.

Table 2: Summary of simulation results for Example 2.

Property	**Case I**	**Case II**
Compression power [MW]	15.19	14.38
F_{MR} [kmol/s]	2.858	2.928
P_{HPR} [MPa]	1.513	1.355
P_{LPR} [MPa]	0.202	0.2065
MHEX 1:		
UA_{MHEX1} [MW/K]	3.07	3.68
$\Delta T_{\text{min,MHEX1}}$ [K]	8.00	8.00
MHEX 2:		
UA_{MHEX2} [MW/K]	7.57	9.50
$\Delta T_{\text{min,MHEX2}}$ [K]	2.50	2.03
$T^{\text{OUT}}_{\text{LPR,MHEX2}}$ [K]	209.91	211.72
Composition [mol %]		
Nitrogen	5.96	5.82
Methane	21.12	20.62
Ethane	40.33	39.37
n-Butane	32.58	34.19

The simulation results for the two cases in Aspen HYSYS are summarized in Table 3. As explained in more detail for Case I, Aspen HYSYS uses different correlations for ideal gas enthalpy calculations leading to shifted driving force distributions compared to Aspen Plus and the nonsmooth model. As observed in Figures 6 and 8, the shift is especially prominent at low temperatures and is likely due to the extrapolation of the enthalpy correlations. The same trend can also be observed in Table 3, in which the calculated UA_{MHEX2}-value deviates considerably from the value obtained by the nonsmooth model.

Table 3: Summary of results from Aspen HYSYS for Example 2.

Property	**Case I**	**Case II**
Compression power [MW]	15.11	14.31
UA_{MHEX1} [MW/K]	2.95	3.54
$\Delta T_{\text{min,MHEX1}}$ [K]	9.34	8.33
UA_{MHEX2} [MW/K]	6.59	8.49
$\Delta T_{\text{min,MHEX2}}$ [K]	3.02	2.04

Example 3

The last example looks at a hybrid version of the two previous processes. As in Example 1, the refrigerant stream is separated at the inlet of the first MHEX and the liquid product is subcooled to $T^{\mathrm{OUT}}_{\mathrm{HPR,MHEX1}}$, throttled and used for precooling the natural gas and the vapor product. The vapor product, on the other hand, is precooled and condensed to $T^{\mathrm{OUT}}_{\mathrm{HPR,MHEX2}}$, throttled and used for cooling the natural gas after NGL extraction. The LPR product from MHEX 2 is mixed with the refrigerant stream from MHEX 1 and used for precooling. The process flowheet is presented in Figure 9.

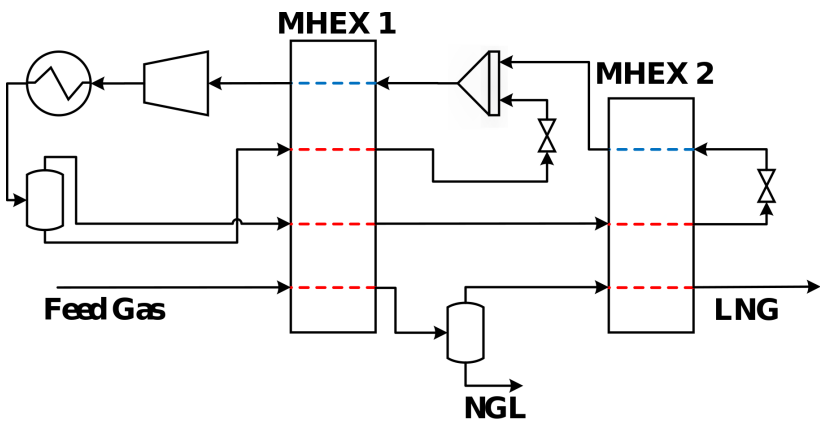

Figure 9: Hybrid process

The refrigerant stream and MHEX data are given in Table S5 in the supporting information. Example 3 uses the same initial refrigerant composition, high and low pressure levels and molar flowrate as in the first example. Furthermore, a rich natural gas composition is chosen to ensure sufficient separation in the NGL separator. The model contains 61 variables, 8 variables more than the process in Example 2 and 18 variables more than the process in Example 1. The model size increases only moderately with additional heat exchangers and refrigerant streams. This is due to the flash calculations and the stream segments in the two-phase region being solved separately from the overall model. Table S6 in the supporting information gives the full set of natural gas stream data used in the simulations. In the model, all hot streams are set to exit the MHEX at the same temperature. Equations (4) and (6) are used to model MHEX 1 as before, whereas Equation (5) is calculated subsequently

during post-processing. As a consequence, the MHEX models can be used to solve for five unknown variables in the process, where the following are considered in the analysis:

- **Case I - variable set**: $T^{\text{OUT}}_{\text{HPR, MHEX1}}$, $\Delta T_{\text{min, MHEX1}}$, P_{HPR}, P_{LPR}, $T^{\text{OUT}}_{\text{LPR, MHEX2}}$.
- **Case II - variable set**: $f_{\text{MR,n-butane}}$, $T^{\text{OUT}}_{\text{LPR, MHEX1}}$, P_{HPR}, $T^{\text{OUT}}_{\text{LPR, MHEX2}}$, UA_{MHEX2}.
- **Case III -variable set**: $T^{\text{OUT}}_{\text{HPR, MHEX1}}$, $T^{\text{OUT}}_{\text{LPR,MHEX1}}$, P_{HPR}, $T^{\text{OUT}}_{\text{LPR,MHEX2}}$, F_{MR}.

Case I. In this case, the minimum approach temperature, the HPR and thus NG temperature out of MHEX 1 (NGL extraction temperature), the high and low pressure levels of the refrigerant as well as the LPR temperature out of MHEX 2 are varied, while keeping the approach temperature and the UA value in MHEX 2 fixed. Changing the NGL extraction temperature is an interesting albeit challenging problem as it determines the LNG composition in MHEX2. The problem is also interesting from an optimization viewpoint as LNG specifications can place constraints on the optimum LNG/NGL split ratio. A solution is obtained with $T^{\text{OUT}}_{\text{HPR, MHEX1}} = 234.99$ K, $\Delta T_{\text{min, MHEX1}} = 1.93$ K, $P_{\text{HPR}} = 1.393$ MPa, $P_{\text{LPR}} = 0.239$ MPa and $T^{\text{OUT}}_{\text{LPR, MHEX2}} = 233.79$ K. The model converged to the solution after 6 iterations and a total simulation time (including initialization) of 38.5 seconds. This solution requires the UA-values for the two exchangers to be $UA_{\text{MHEX1}} = 6.43$ MW/K and $UA_{\text{MHEX2}} = 9.00$ MW/K, respectively. The resulting isentropic compression power for the nonsmooth solution was 13.30 MW.

Figure 10 presents the hot and cold composite curves in each MHEX. A direct comparison with the results from Example 1 is not possible as the HPR temperature out of MHEX 1 is treated implicitly in the first example. Moreover, the model only solves for three variables, compared to five variables in this case, and thus two additional stream variables must be fixed in Example 1. Nevertheless, the composite curves show a similar trend as for the results in Figures 2a and 3a. The curves approach one-another at three distinct locations resulting in the two peaks in Figure 11b that can also be observed in Figures 2b and 3b.

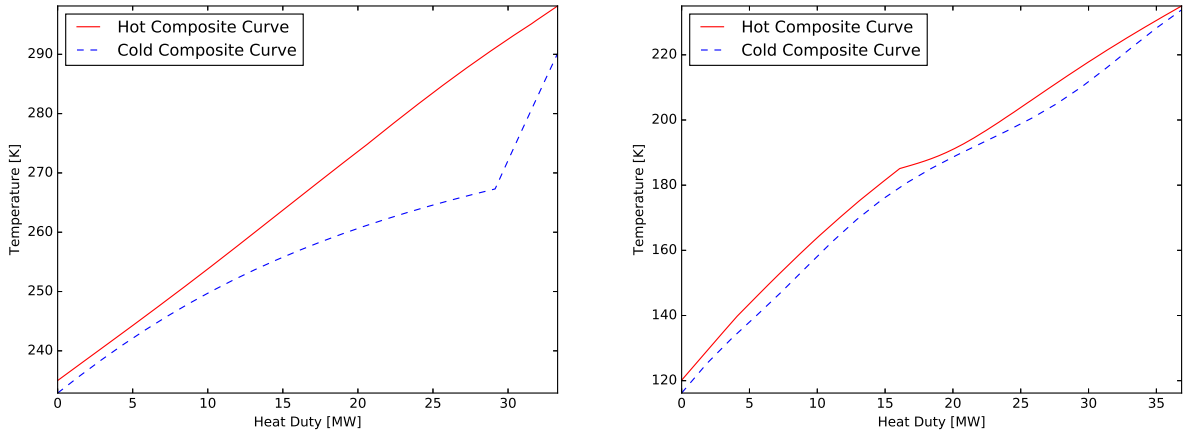

(a) (b)

Figure 10: (a.) Composite curves for MHEX 1 in Example 3, Case I. (b.) Corresponding for MHEX 2.

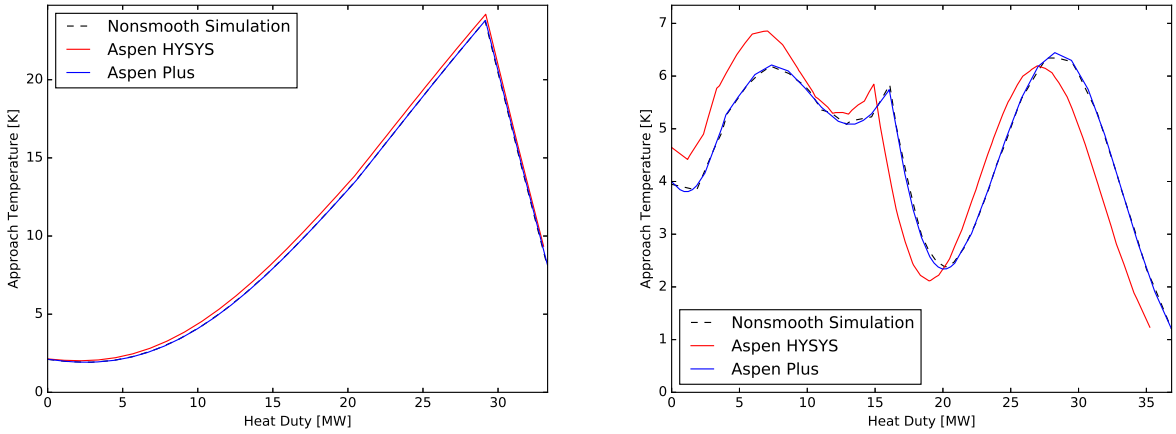

(a) (b)

Figure 11: (a.) Driving force plot for MHEX 1 in Example 3, Case I. (b.) Corresponding for MHEX 2.

The same process was simulated with Aspen Plus and Aspen HYSYS using the solution from the nonsmooth model as input and letting the LPR outlet temperature vary in both MHEXs. The driving force plots are presented along with the results from the nonsmooth simulation in Figure 11. Simulations in Aspen Plus resulted in an isentropic compression power requirement of 13.29 MW. The UA-values are $UA_{\text{MHEX1}} = 6.44$ MW/K and $UA_{\text{MHEX2}} = 9.04$ MW/K, both within 1% of the values determined by the nonsmooth model. Furthermore, $\Delta T_{\text{min,MHEX1}} = 1.93$ K and $\Delta T_{\text{min,MHEX2}} = 1.21$ K, whereas the respective values for the nonsmooth model are $\Delta T_{\text{min,MHEX1}} = 1.93$ K and $\Delta T_{\text{min,MHEX2}} = 1.20$ K. A summary of the HYSYS results is found in Table 5.

Case II. The second case varies the refrigerant composition, temperature into the compressor, the high pressure level, the LPR temperature out of MHEX 2 and the UA_{MHEX2}-value. The approach temperatures were set to $\Delta T_{\text{min,MHEX1}} = 5.00$ K and $\Delta T_{\text{min,MHEX2}} = 0.75$ K. The model converged after 6 iterations and a total simulation time (with initialization) of 48.1 seconds to a solution with $T^{\text{OUT}}_{\text{LPR, MHEX1}} = 273.72$ K, $T^{\text{OUT}}_{\text{LPR, MHEX2}} = 247.29$ K, $P_{\text{HPR}} = 1.352$ MPa and $UA_{\text{MHEX2}} = 13.75$ MW/K. At the specified approach temperature in MHEX 1, the UA_{MHEX1}-value was calculated to be 2.01 MW/K. The new refrigerant composition consists of 5.51 % nitrogen, 19.52 % methane, 37.27 % ethane and 37.70 % n-butane with $F_{\text{MR}} = 3.093$ kmol/s. Figure 12 presents the hot and cold composite curves for the process. This solution resulted in an isentropic compression power of 14.35 MW.

Figure 13 presents the driving force plots for the nonsmooth, Aspen Plus and Aspen HYSYS simulations in Case II. As before, Aspen Plus and the nonsmooth model obtain nearly identical results. The isentropic power requirement is 14.34 MW. In addition, the UA values of the two MHEXs are $UA_{\text{MHEX1}} = 2.01$ MW/K and $UA_{\text{MHEX2}} = 14.236$ MW/K. The corresponding values for the nonsmooth model are $UA_{\text{MHEX1}} = 2.01$ MW/K and $UA_{\text{MHEX2}} = 13.75$ MW/K. The approach temperatures in the two MHEXs are $\Delta T_{\text{min,MHEX1}} = 4.99$ K compared to 5.00 K fixed in the nonsmooth model and $\Delta T_{\text{min,MHEX2}} = 0.71$ K compared to 0.75 K for the nonsmooth model. The results from Aspen HYSYS are presented in Table 5.

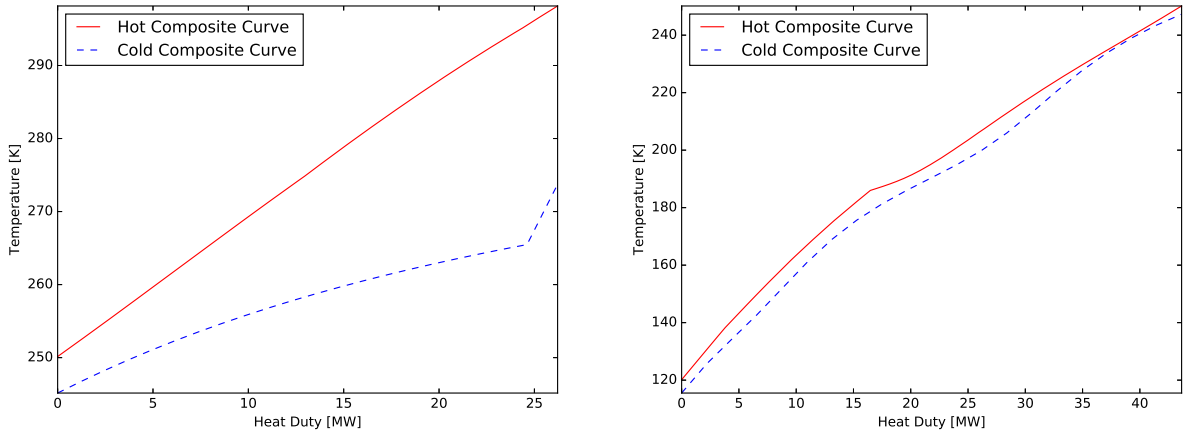

(a) (b)

Figure 12: (a.) Composite curves for MHEX 1 in Example 3, Case II. (b.) Corresponding for MHEX 2.

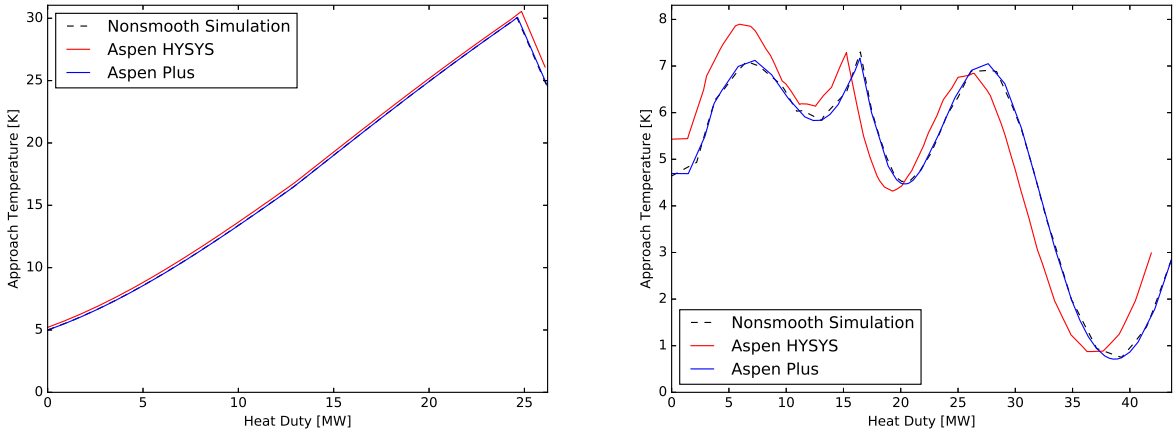

(a) (b)

Figure 13: (a.) Driving force plot for MHEX 1 in Example 3, Case II. (b.) Corresponding for MHEX 2.

Case III. The last case solves for the HPR and thus NG temperature out of MHEX 1, the temperature into the compressor, the HPR pressure level, the LPR temperature out of MHEX 2 as well as the refrigerant flowrate. The flowsheet converged after 57.5 seconds and 9 iterations to a solution with $T^{\text{OUT}}_{\text{HPR, MHEX1}} = 245.80$ K, $T^{\text{OUT}}_{\text{LPR,MHEX1}} = 284.74$ K, $P_{\text{HPR}} = 1.565$ MPa, $T^{\text{OUT}}_{\text{LPR,MHEX2}} = 243.66$ K and $F_{\text{MR}} = 2.808$ kmol/s. In addition, the UA_{MHEX1} value at the solution is 2.15 MW/K, and the required isentropic compression power is 14.85 MW. The composite curves for the process are provided in Figure 14. A summary of the results for the three simulation cases is presented in Table 4.

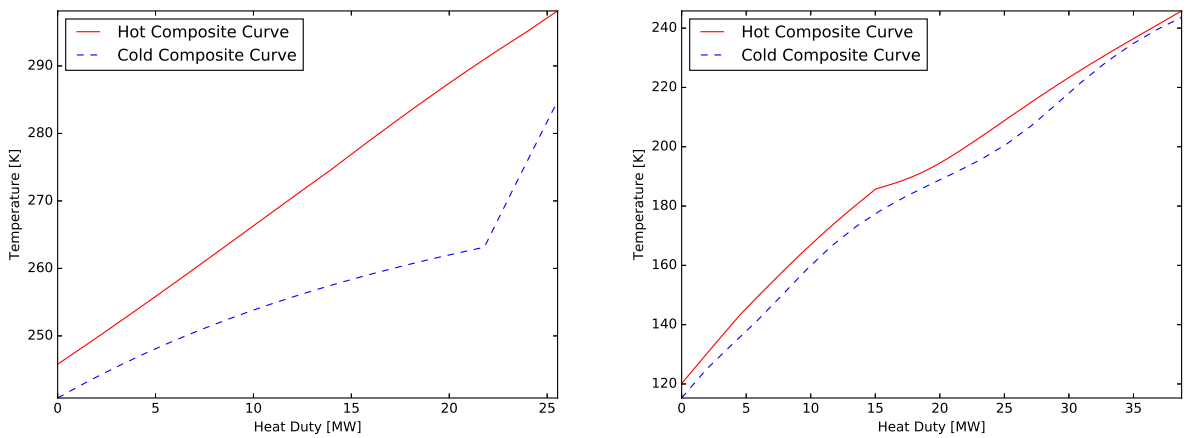

(a) (b)

Figure 14: (a.) Composite curves for MHEX 1 in Example 3, Case III. (b.) Corresponding for MHEX 2.

The driving force plots for the nonsmooth model along with the results from Aspen Plus and Aspen HYSYS model are provided in Figure 15. The graphs show similar tendencies to what was observed in the two previous cases. Aspen Plus displays a nearly identical driving force distribution as the nonsmooth model, whereas the solution from Aspen HYSYS deviates from the other models at low temperatures. Aspen Plus calculates an isentropic compression power requirement of 14.84 MW. The UA-values are $UA_{\text{MHEX1}} = 2.15$ MW/K and $UA_{\text{MHEX2}} = 8.63$ MW/K, with $\Delta T_{\text{min,MHEX1}} = 4.99$ K and $\Delta T_{\text{min,MHEX2}} = 1.45$ K. The corresponding values for the nonsmooth model are $UA_{\text{MHEX1}} = 2.15$ MW/K, $UA_{\text{MHEX2}} =$

8.50 MW/K, $\Delta T_{\text{min,MHEX1}} = 5.00$ K and $\Delta T_{\text{min,MHEX2}} = 1.50$ K.

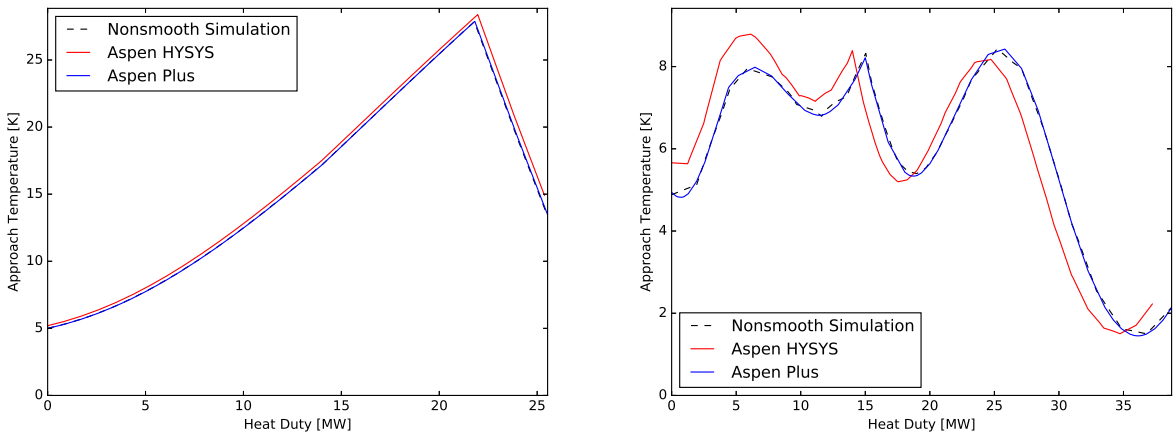

(a) (b)

Figure 15: (a.) Driving force plot for MHEX 1 in Example 3, Case III. (b.) Corresponding for MHEX 2.

Table 5 presents the results of the three cases in Aspen HYSYS. As in Example 2, Aspen HYSYS calculates a different driving force distribution than Aspen Plus and the nonsmooth model, which is a result of different correlations used for ideal gas enthalpy calculations. This mostly affect the calculations at low temperatures.

Conclusions

This paper has presented an application of the nonsmooth flowsheeting strategy developed by Watson et al.[14] for simulating three single mixed refrigerant processes of different complexity with the Peng-Robinson equation of state. Different cases for each process were analyzed, and the simulations were performed by solving an algebraic equation system using a nonsmooth Newton-type solver provided with exact sensitivity information in the form of generalized derivative elements. Various sets of unknown variables were considered in the analysis to study whether the nonsmooth model converged to feasible solutions. Few iterations were required to solve for each case and the results correlate well with values obtained from Aspen

Table 4: Summary of simulation results for Example 3.

Property	**Case I**	**Case II**	**Case III**
Compression power [MW]	13.30	14.35	14.85
F_{MR} [kmol/s]	2.928	3.093	2.808
P_{HPR} [MPa]	1.393	1.352	1.565
P_{LPR} [MPa]	0.239	0.202	0.202
MHEX 1:			
UA_{MHEX1} [MW/K]	6.43	2.01	2.15
$\Delta T_{\mathrm{min,MHEX1}}$ [K]	1.93	5.00	5.00
$T^{\mathrm{OUT}}_{\mathrm{HPR,MHEX1}}$ [K]	234.99	250.15	245.80
$T^{\mathrm{OUT}}_{\mathrm{LPR,MHEX1}}$ [K]	290.15	273.72	284.79
MHEX 2:			
UA_{MHEX2} [MW/K]	9.00	13.75	8.50
$\Delta T_{\mathrm{min,MHEX2}}$ [K]	1.20	0.75	1.50
$T^{\mathrm{OUT}}_{\mathrm{LPR,MHEX2}}$ [K]	233.79	247.29	243.66
Composition [mol %]			
Nitrogen	5.82	5.51	5.82
Methane	20.62	19.52	20.62
Ethane	39.37	37.27	39.37
n-Butane	34.19	37.70	34.19

Table 5: Summary of results from Aspen HYSYS for Example 3.

Property	**Case I**	**Case II**	**Case III**
Compression power [MW]	13.23	14.27	14.76
UA_{MHEX1} [MW/K]	6.07	1.95	2.07
$\Delta T_{\mathrm{min,MHEX1}}$ [K]	2.02	5.21	5.19
UA_{MHEX2} [MW/K]	8.68	12.70	8.08
$\Delta T_{\mathrm{min,MHEX2}}$ [K]	1.24	0.88	1.51

Plus. The nonsmooth model also managed to locate feasible solutions for more challenging problems, such as varying the refrigerant compositions that impact large portions of the flowsheet. On the other hand, both Aspen Plus and Aspen HYSYS were unable to solve these challenging problems, instead only being able to validate the results of the nonsmooth simulation. This versatility makes the software suitable for simulation, as well as a basis for optimization. Validations performed by Aspen HYSYS achieved similar results as the nonsmooth model at high temperatures but deviated from the solution at lower temperatures. The disparity in the solutions is caused by the nonsmooth models and Aspen Plus using another ideal gas enthalpy correlation than HYSYS. In particular, this affected the total duty and calculated area of the low temperature MHEX in the models, which emphasizes the importance of matching the physical property correlations before comparing simulation and optimization results from different models. As stream segments for the two-phase region are handled separately in nested subroutines and the size of the pinch location algorithm remains unchanged irrespective of the number of stream segments, the model size increases only moderately with additional streams and heat exchangers. This makes the nonsmooth framework suitable for handling larger and more complex LNG liquefaction processes. The authors plan to include the models discussed in this paper in an optimization framework. The nonsmooth framework will also be used for simulation and optimization of dual mixed refrigerant processes.

Supporting Information Available

Process stream data and initial guess values for the simulations in Examples 1, 2 and 3.

Acknowledgement

This publication has been funded by HighEFF – Centre for an Energy Efficient and Competitive Industry for the Future. The authors gratefully acknowledge the financial support from

the Research Council of Norway and user partners of HighEFF, an 8 year Research Centre under the FME scheme (Centre for Environment-friendly Energy Research, 257632/E20). Harry A. J. Watson acknowledges Statoil for providing funding for this project.

Nomenclature

Roman letters

$\mathcal{C}^1$	=	class of continuously differentiable functions
EBP	=	enthalpies of the extended composite curves [W]
$\mathbf{f}'(\mathbf{x};\mathbf{M})$	=	lexicographic derivative of $\mathbf{f}$ at $\mathbf{x}$ in directions $\mathbf{M}$
f	=	component molar flowrate [mol/s]
F	=	total molar flowrate [mol/s]
$\mathbf{G}$	=	element of generalized derivative
K	=	equilibrium coefficient
mC_{p}	=	heat capacity flowrate [W/K]
$\mathbf{M}$	=	directions matrix
n_{c}	=	total number of components
T	=	temperature [K]
UA	=	heat exchanger conductance [W/K]
P	=	absolute pressure [Pa]
$\mathcal{PC}^1$	=	class of piecewise differentiable functions
Q	=	heat duty [W]
$\mathbf{y}$	=	equation residuals
z	=	mole fraction

Greek letters

α	=	vapor fraction
β	=	user-defined parameter in smooth approximation

ΔT_{LM} = log mean temperature difference [K]

ΔT_{min} = minimum approach temperature [K]

ΔQ = enthalpy change [W]

γ = variable in the LP-Newton

Subscripts and superscripts

2p = two-phase substream

BP = bubble point

C = cold stream

DP = dew point

in/out = inlet/outlet temperature of a substream

IN/OUT = inlet/outlet temperature of a process stream

H = hot stream

HPR = high pressure refrigerant

LPR = low pressure refrigerant

MHEX1/2 = multistream heat exchanger 1/2

MR = mixed refrigerant

p = pinch candidate

sub = subcooled substream

sup = superheated substream

References

(1) Hwang, J.-H.; Ku, N.-K.; Roh, M.-I.; Lee, K.-Y. Optimal Design of Liquefaction Cycles of Liquefied Natural Gas Floating, Production, Storage, and Offloading Unit Considering Optimal Synthesis. *Industrial & Engineering Chemistry Research* **2013**, *52*, 5341–5356.

(2) Lim, W.; Choi, K.; Moon, I. Current Status and Perspectives of Liquefied Natural Gas

(LNG) Plant Design. *Industrial & Engineering Chemistry Research* **2013**, *52*, 3065–3088.

(3) *Aspen Technology Inc., Aspen Plus v9*; Aspen Technology Inc.: Bedford, MA, 2016.

(4) *Aspen Technology Inc., Aspen HYSYS v9*; Aspen Technology Inc.: Bedford, MA, 2016.

(5) Kamath, R. S.; Biegler, L. T.; Grossmann, I. E. Modeling multistream heat exchangers with and without phase changes for simultaneous optimization and heat integration. *AIChE Journal* **2012**, *58*, 190–204.

(6) Watson, H. A. J.; Khan, K. A.; Barton, P. I. Multistream heat exchanger modeling and design. *AIChE Journal* **2015**, *61*, 3390–3403.

(7) Hasan, M. M. F.; Karimi, I. A.; Alfadala, H.; Grootjans, H. Modeling and simulation of main cryogenic heat exchanger in a base-load liquefied natural gas plant. *Computer Aided Chemical Engineering* **2007**, *24*, 219–224.

(8) Hasan, M. M. F.; Karimi, I. A.; Alfadala, H.; Grootjans, H. Operational modeling of multistream heat exchangers with phase changes. *AIChE Journal* **2009**, *55*, 150–171.

(9) Rao, H. N.; Karimi, I. A. A superstructure-based model for multistream heat exchanger design within flow sheet optimization. *AIChE Journal* **2017**, *63*, 3764–3777.

(10) Duran, M. A.; Grossmann, I. E. Simultaneous optimization and heat integration of chemical processes. *AIChE Journal* **1986**, *32*, 123–138.

(11) Pattison, R. C.; Baldea, M. Multistream heat exchangers: Equation-oriented modeling and flowsheet optimization. *AIChE Journal* **2015**, *61*, 1856–1866.

(12) Watson, H. A. J.; Vikse, M.; Gundersen, T.; Barton, P. I. Optimization of single mixed-refrigerant natural gas liquefaction processes described by nondifferentiable models. Submitted.

(13) Watson, H. A. J.; Barton, P. I. Modeling phase changes in multistream heat exchangers. *International Journal of Heat and Mass Transfer* **2017**, *105*, 207–219.

(14) Watson, H. A. J.; Vikse, M.; Gundersen, T.; Barton, P. I. Reliable Flash Calculations: Part 2. Process flowsheeting with nonsmooth models and generalized derivatives. *Industrial & Engineering Chemistry Research* **In press**,

(15) Rachford, H. H.; Rice, J. D. Procedure for Use of Electronic Digital Computers in Calculating Flash Vaporization Hydrocarbon Equilibrium. *Journal of Petroleum Technology* **1952**, *4*, 327–328.

(16) Boston, J. F.; Britt, H. I. A radically different formulation and solution of the single-stage flash problem. *Computers & Chemical Engineering* **1978**, *2*, 109–122.

(17) Watson, H. A. J.; Vikse, M.; Gundersen, T.; Barton, P. I. Reliable Flash Calculations: Part 1. Nonsmooth Inside-Out Algorithms. *Industrial & Engineering Chemistry Research* **2017**, *56*, 960–973.

(18) Watson, H. A. J.; Barton, P. I. Reliable Flash Calculations: Part 3. A nonsmooth approach to density extrapolation and pseudoproperty evaluation. *Industrial & Engineering Chemistry Research* **In press**,

(19) Balakrishna, S.; Biegler, L. T. Targeting strategies for the synthesis and energy integration of nonisothermal reactor networks. *Industrial & engineering chemistry research* **1992**, *31*, 2152–2164.

(20) Grossmann, I. E.; Yeomans, H.; Kravanja, Z. A rigorous disjunctive optimization model for simultaneous flowsheet optimization and heat integration. *Computers & Chemical Engineering* **1998**, *22*, 157–164.

(21) Facchinei, F.; Fischer, A.; Herrich, M. An LP-Newton method: nonsmooth equations, KKT systems, and nonisolated solutions. *Mathematical Programming* **2014**, *146*, 1–36.

(22) Fischer, A.; Herrich, M.; Izmailov, A. F.; Solodov, M. V. A Globally Convergent LP-Newton Method. *SIAM Journal on Optimization* **2016**, *26*, 2012–2033.

(23) Clarke, F. H. *Optimization and Nonsmooth Analysis*; SIAM: Philadelphia, PA, 1990.

(24) Nesterov, Y. Lexicographic differentiation of nonsmooth functions. *Mathematical Programming* **2005**, *104*, 669–700.

(25) Khan, K. A.; Barton, P. I. Generalized Derivatives for Solutions of Parametric Ordinary Differential Equations with Non-differentiable Right-Hand Sides. *Journal of Optimization Theory and Applications* **2014**, *163*, 355–386.

(26) Khan, K. A.; Barton, P. I. A vector forward mode of automatic differentiation for generalized derivative evaluation. *Optimization Methods and Software* **2015**, *30*, 1185–1212.

(27) Barton, P. I.; Khan, K. A.; Stechlinski, P.; Watson, H. A. J. Computationally relevant generalized derivatives: theory, evaluation and applications. *Optimization Methods & Software* **In press**,

(28) Scholtes, S. *Introduction to piecewise differentiable equations*, 1st ed.; SpringerBriefs in Optimization: New York, 2012.

(29) Facchinei, F.; Pang, J.-S. *Finite-Dimensional Variational Inequalities and Complementarity Problems*, vol. 2 ed.; Springer-Verlag New York, Inc.: New York, NY, 2003.

(30) Aly, F. A.; Lee, L. L. Self-consistent equations for calculating the ideal gas heat capacity, enthalpy, and entropy. *Fluid Phase Equilibria* **1981**, *6*, 169–179.

Graphical TOC Entry